# Tight-binding study of grain boundaries in Si: Energies and atomic structures of twist grain boundaries

Masanori Kohyama
*Department of Material Physics, Osaka National Research Institute, Agency of Industrial Science and Technology, 1-8-31 Midorigaoka, Ikeda, Osaka 563, Japan*

Ryoichi Yamamoto
*Institute of Industrial Science, University of Tokyo, 7-22-1 Roppongi, Minato-ku, Tokyo 106, Japan*
(Received 8 November 1993; revised manuscript received 14 February 1994)

The overall features of the energies and atomic structures of the twist boundaries in Si have been examined by energy-minimization calculations using the transferable semiempirical tight-binding method, and the results have been compared with those of the tilt boundaries in Si. First, the $\{122\}\Sigma=9$ tilt boundary has been dealt with as a typical tilt boundary observed in polycrystalline Si. It has been shown that the configuration consisting of atomic rings without any coordination defects can exist stably with a relatively small interfacial energy, 0.32 J/m$^2$, and with small bond-length and bond-angle distortions within about $\pm 2\%$ and about $\pm 20°$, similarly to the other tilt boundaries. The twist boundaries with different rotation axes and boundary planes, the $\langle 111\rangle$ $\Sigma=7$, $\langle 011\rangle$ $\Sigma=3$, and $\langle 001\rangle$ $\Sigma=5$ twist boundaries, have been examined against various rigid-body translations parallel to the interface. It has been found that the twist boundaries contain larger bond distortions or more coordination defects, and much larger interfacial energies than those of the tilt boundaries, at least when they are constructed by ideal surfaces. It seems that there do not exist deep or sharp energy minima against the rigid-body translations, differently from the tilt boundaries. About the $\langle 111\rangle$ $\Sigma=7$ and $\langle 011\rangle$ $\Sigma=3$ boundaries, configurations without any coordination defects can be constructed for proper translations. However, in the $\langle 111\rangle$ $\Sigma=7$ boundaries, large bond stretchings are inevitably introduced except at the sites of good coincidence, and the $\langle 011\rangle$ $\Sigma=3$ boundary frequently contains four-membered rings with large bond-angle distortions. Thus the most stable configurations of these boundaries contain interfacial energies over three times larger than the value of the $\Sigma=9$ tilt boundary, and contain shallow states in the band gap. On the other hand, the $\langle 001\rangle$ $\Sigma=5$ boundaries have very complex structures as compared with the other twist boundaries. The interfacial energies are much larger than the other twist boundaries, the configurations frequently contain coordination defects and deep states in the band gap, and there seem to exist many metastable configurations with different bonding networks in a similar energy range, similarly to the results of the same boundaries in Ge by Tarnow *et al.* [Phys. Rev. B **42**, 3644 (1990)]. The present different features of the respective twist boundaries can be explained by the morphology of the respective ideal surfaces. It can be said that stable configurations of the tilt boundaries and other extended defects in Si or Ge are constructed by arranging the structural units consisting of atomic rings without any large bond distortions or coordination defects. For twist boundaries, such stable structural units cannot be easily constructed, which causes the present greater structural disorder and larger interfacial energies. This is the reason why twist boundaries are seldom found in polycrystalline Si as compared with the frequently observed tilt boundaries.

## I. INTRODUCTION

Studies of grain boundaries in semiconductors are of much importance in order to understand the properties of polycrystalline semiconductors applied to solar cells or various electronic devices such as thin film transistors (TFT's).[1] Disordered structures at grain boundaries often strongly affect the electronic properties of semiconductors through the generation of shallow or deep states in the band gap, or through interactions with impurities or dopants. Grain boundaries in semiconductors are also of interest as typical examples of grain boundaries in covalent crystals as compared with those in metals or in ionic crystals.[2] The understanding of grain boundaries in covalent crystals is very important for the development of the high performance covalent ceramics such as SiC, AlN, or $Si_3N_4$, where grain boundaries dominate various properties of ceramics such as sintering, mechanical, chemical, and electronic properties.

In general, grain boundaries in crystals can be classified and analyzed geometrically by the concepts of tilt and twist boundaries and of the coincidence site lattice (CSL).[3] Tilt and twist boundaries are geometrical extremes of grain boundaries defined by the relation between the rotation axis and the boundary plane, although general boundaries contain both tilt and twist components. The CSL is the intersection of the lattices of two grains, and the coincidence index $\Sigma$ is the reciprocal density of coincidence lattice sites with respect to the original lattice. The periodicity of the boundary structure can be analyzed by the periodicity in the plane in the CSL. CSL boundaries with relatively small $\Sigma$ values con-

 ©1994 The American Physical Society

tain short periods, and can be formed for singular rotation angles.

Nowadays, it is of considerable importance to understand the structure and properties of grain boundaries in materials from a microscopic viewpoint beyond the geometric viewpoint described above, because the energies and properties of boundaries are primarily dominated by atomic and electronic structures of interfaces, which finally depend on the bonding nature of materials. It is also important to clarify the dependence of the properties of boundaries on the geometric conceptions, through the understanding of atomic and electronic structures.

Concerning grain boundaries in semiconductors, significant advances have been made in the experimental and theoretical understanding of the tilt boundaries in elemental semiconductors such as Si or Ge.[4-6] The symmetrical tilt grain boundaries exist frequently in polycrystalline Si or Ge, and these are usually CSL boundaries. Many high-resolution transmission electron microscopy (HRTEM) observations[7-12] have indicated that such tilt boundaries are constructed by arrangement of the structural units consisting of atomic rings without any coordination defects. Energy-minimization calculations[11,13] have shown the stability of such configurations and the applicability of the structural unit model[14] to such configurations. More quantitatively, theoretical calculations using the tight-binding method[15-19] or the first-principles density-functional method[20-22] have proved that such configurations of the CSL tilt boundaries in Si or Ge are stable with no false local energy minima, and that such configurations contain no electronic states inside the minimum band gap between the bulk valence-band maximum and the bulk conduction-band minimum, although the boundary-localized states are frequently generated at the band edges. These points are consistent with the experiments, indicating that the CSL tilt boundaries in Si or Ge are intrinsically electrically nonactive.[5]

However, there exist many experiments indicating the presence of band tails[23-26] or midgap states[26] at grain boundaries in Si. It can be considered[1,5,27,28] that these gap states should be associated with general disordered grain boundaries containing greater structural disorder than the observed CSL tilt boundaries, or with defects in the CSL tilt boundaries, or with segregated or precipitated impurities or dopants. As the next step, one of the most important subjects is to elucidate the origins of such band tails or midgap states at grain boundaries from a microscopic viewpoint.

On the other hand, there have been relatively few studies of twist boundaries in semiconductors. Experimentally, twist boundaries are seldom found in polycrystalline Si or Ge as compared with the tilt boundaries, and little is known about stable atomic configurations. Thus there remain basic questions such as why twist boundaries are seldom found in Si or Ge as compared with tilt boundaries, or what atomic configurations twist boundaries contain.

Several theoretical calculations have indicated that twist boundaries in Si or Ge have fairly different features from those of tilt boundaries. We examined the configurations and energies of various CSL $\langle 111 \rangle$ twist boundaries in Si (Ref. 29) by using the bond orbital model, which corresponds to an angularly dependent interatomic potential for tetrahedral semiconductors based on the tight-binding approximation.[13] The twist boundaries are constructed by two ideal (111) surfaces, and configurations without any coordination defects are at least quasistable. However, the densities of bond distortions and interfacial energies are very large compared with the tilt boundaries. Phillpot and Wolf[30] also performed energy-minimization calculations for several types of twist boundaries in Si using the Stillinger-Weber potential,[31] which is an empirical interatomic potential for Si. They obtained configurations with greater structural disorder and larger interfacial energies than the tilt boundaries. More quantitatively, Tarnow *et al.*[32] performed energy-minimization calculations for the $\langle 011 \rangle$ $\Sigma=5$ twist boundaries in Ge by using the *ab initio* pseudopotential method. They examined the overall features of energies and atomic structures against the rigid-body translations, and found that there are no sharp or deep energy minima against the translations parallel to the interface in contrast to the tilt boundaries.[33] The interfaces contain many distorted or weak bonds and coordination defects, which cause very large interfacial energies and gap states.

The first aim of the present study is to examine the overall features of the energies and atomic structures of various twist boundaries in Si as compared with the tilt boundaries, and to investigate the reason why twist boundaries are seldom found in polycrystalline Si. We deal with the $\langle 111 \rangle$ $\Sigma=7$, $\langle 011 \rangle$ $\Sigma=3$, and $\langle 001 \rangle$ $\Sigma=5$ twist boundaries in Si, which are typical CSL twist boundaries containing three types of rotation axes and boundary planes. Energy-minimization calculations are performed with respect to various rigid-body translations between the two grains. We use the transferable semiempirical tight-binding (SETB) method,[34,35] which can give atomic and electronic structures and energies of various systems of Si more correctly than the usual SETB method.[36] For comparison, we also deal with a typical symmetrical tilt boundary, the $\{122\}$ $\Sigma=9$ tilt boundary in Si, by using the same theoretical method. The $\langle 001 \rangle$ twist boundaries in Si and the $\langle 111 \rangle$ and $\langle 011 \rangle$ twist boundaries in semiconductors have not been sufficiently examined quantum-mechanically to date. For greatly distorted systems of Si such as twist boundaries, electronic structure calculations are essential in order to obtain reliable results as compared with empirical potentials such as the Stillinger-Weber potential.

As will be shown, the present results indicate that twist boundaries in Si contain more distorted bonds or coordinated defects and larger interfacial energies than the observed tilt boundaries, and that stable structural units without any large bond distortions or coordination defects such as those in the tilt boundaries cannot be easily constructed for twist boundaries. This is the reason why twist boundaries are seldom found in polycrystalline semiconductors, as compared with tilt boundaries.

The second aim of the present study is to examine the

electronic structures of twist boundaries in Si as compared with those of the tilt boundaries, and to investigate the relations between the structural disorder and the electronic structure at interfaces. As will be shown, the twist boundaries contain various kinds of structural disorder or coordination defects, and these frequently introduce shallow or deep states in the band gap. Such local structural disorder and gap states should be common to those in general disordered boundaries in Si, and should be the origins of the observed band tails or midgap states in polycrystalline Si mentioned above. It should be noted that the study of twist boundaries should contribute to an understanding of general disordered boundaries containing gap states.

In the present paper, we primarily report results for the energies and atomic structures of twist boundaries in Si, and discuss the overall features of those of the twist boundaries. The detailed analyses of the electronic structures will be given in our following papers.[37] The present paper is organized as follows. In Sec. II, the theoretical method and computational scheme are described. In Sec. III, the models and supercells of the $\langle 111 \rangle$ $\Sigma=7$, $\langle 011 \rangle$ $\Sigma=3$, and $\langle 001 \rangle$ $\Sigma=5$ twist boundaries are presented, and the rigid-body translations are defined. In Sec. IV, results of energy-minimization calculations for the tilt boundary and twist boundaries are reported and analyzed. Section V discusses features of the energies and atomic structures of the twist boundaries in Si as compared with the tilt boundaries.

## II. METHOD OF CALCULATIONS

### A. The transferable SETB method

We use the transferable SETB method[34,35] coupled with the supercell technique. The usual SETB method[36] deals with atomic and electronic structures and energies of complex systems of Si containing a large number of atoms, and has been shown to be quite useful for calculations of the symmetrical tilt boundaries in Si.[15–20] However, the SETB method is less reliable for systems containing greatly distorted bonds or coordination defects, because the transferability for structures other than four-coordinated ones is not necessarily guaranteed.[16,38] The transferable SETB method has been developed in order to overcome this problem, and can reproduce properly the binding energies and equilibrium volumes of variously coordinated structures of Si. Thus this method is applicable to greatly distorted systems such as twist boundaries.

In this method, the binding energy of the system, which is the difference between the total energy of the system and that of the isolated atoms, is expressed as a sum of the band-structure energy $E_{\rm bs}$ and the remaining repulsive energy $E_{\rm rep}$. $E_{\rm bs}$ is a sum of occupied eigenenergies by a tight-binding band-structure calculation with a valence atomic orbital basis, and $E_{\rm rep}$ is expressed as a sum of short-range interatomic repulsive potentials, in the same way as the usual SETB method. However, differently from the usual SETB method, the behavior of the two-center hopping integrals $V_{ll'm}(r)$ in the tight-binding Hamiltonian and that of the repulsive interatomic potential $\varphi(r)$ are modified for large distances, and these are smoothly truncated by attenuation functions $S(r)$ as

$$V_{ll'm}(r)=\eta_{ll'm}S(r)r^{-\nu} \tag{1}$$

and

$$\varphi(r_{ij})=A_{ij}S(r_{ij})r_{ij}^{-\nu} , \tag{2}$$

where

$$S(r)=1/\{1+\exp[\mu(r-R_c)]\} . \tag{3}$$

$\eta_{ll'm}$, $\nu$, $\mu$, and $R_c$ are the parameters.

The present method has two characteristics as compared with the other type of transferable method.[38] The first is that different values of $\nu$, $\mu$, and $R_c$ are used for respective hopping integrals. Different exponent values were selected following the work by Robertson,[39] and the other parameters for the Hamiltonian were determined so as to reproduce the first- and second-neighbor integrals in the Hamiltonian of diamond Si given by Pandey and Phillips.[40]

The second characteristic is that the interatomic repulsive potential has a dependence on the local environment through the effective coordination numbers. $A_{ij}$ in Eq. (2) is given as

$$A_{ij}=b_0-b_1(Z_i+Z_j) . \tag{4}$$

$Z_i$ is the effective coordination number of the atom $i$, and is given by

$$Z_i=\sum_{j\neq i}\exp[-\lambda_1(r_{ij}-R_i)^2] , \tag{5}$$

where

$$R_i=\sum_{j\neq i} r_{ij}e^{-\lambda_2 r_{ij}}\left[\sum_{j\neq i} e^{-\lambda_2 r_{ij}}\right]^{-1} . \tag{6}$$

$b_0$, $b_1$, $\lambda_1$, and $\lambda_2$ are the parameters. All the parameters for the repulsive potential were determined so as to reproduce the binding energies and equilibrium volumes of various phases of Si, including the dimer.

As shown in Ref. 35, these two points much improve the representation of the atomic and electronic structures and energies of various phases of Si as compared with the other transferable method.[38] The Hamiltonian, including the interactions beyond the first neighbors, is suited to various configurations, and the incorporation of the dependence on the local environment into the repulsive energy is especially important for the transferability. The overlap interaction between the basis orbitals that is neglected in the calculation of $E_{\rm bs}$ in the SETB method is one of the origins of the repulsive energy $E_{\rm rep}$. Strictly, this interaction depends on the local environment through the overlap matrix coupled with the Hamiltonian. Thus this effect cannot be included properly in $E_{\rm rep}$ by a simple sum of interatomic repulsive potentials as in the usual method.

All parameters used in the present study are listed in Table I. As described in Ref. 35, we have made readjustments of the two parameters $b_0$ and $b_1$, as compared with the original values.[34] These have been determined so as to reproduce more correctly the binding energies and equilibrium volumes of variously coordinated structures of Si, with natural truncation of the interactions by the attenuation functions of Eq. (3), although the interactions after the second neighbors are artificially truncated in Ref. 34.

Additionally, we have examined the applicability of the present method with the new parameters to graphitic Si as a three-coordinated structure, because the applicability only to overcoordinated structures is examined in Ref. 35. The binding energy and equilibrium structure of a sheet of graphitic Si have been calculated by using 18 special-**k** points,[41] because the interlayer distance[42] is large enough for the present method. The calculated equilibrium bond length is 2.197 Å, and the energy increase against the diamond structure is 0.63 eV/atom. It can be said that the present results are in fairly good agreement with the *ab initio* results, 2.249 Å and 0.71 eV/atom.[42]

Thus it can be assumed that the present method can deal with complex systems of Si containing overcoordinated or undercoordinated atoms relatively correctly, and with relatively short computing time. A shortcoming of the present method is the overestimation of the width of the bulk band gap as 2.2 eV. The conduction band of the perfect crystal of Si is reproduced to be shifted upward by about 0.7 eV by the present parameters. This problem seems to be caused by the truncation of the interactions in determining the parameters in Ref. 34. However, the valence band and the shape of the dispersion of the lower part of the conduction band can be as well reproduced as those in Ref. 40.

### B. Electrostatic interactions

In the present calculations, the intra-atomic electrostatic interactions are included self-consistently through the form of a Hubbard-like Hamiltonian. This should be important for greatly distorted systems in order to suppress unrealistic large charge transfers between atoms. In this scheme, an on-site electron-repulsion term

$$H_u = \frac{1}{2} U \sum_i (n_i - n_i^0)^2 \tag{7}$$

is added to the binding energy of the system. $n_i$ is the total valence occupancy of the atom $i$, and $n_i^0$ is that in the perfect crystal, namely 4. In the Hamiltonian for the electronic structure, the term $U(n_i - n_i^0)$ is added to the respective on-site terms, and the one-electron equation of the Hamiltonian is solved self-consistently. The intra-atomic interactions are summed up in $E_{\rm bs}$, and are finally included in the binding energy as the form of Eq. (7) by adjusting the total sum in $E_{\rm bs}$. For the parameter, we use $U = 2.0$ eV, which corresponds to the value used for Si clusters in Ref. 43.

In the usual SETB method, electrostatic interactions are not dealt with explicitly. Recently, it has been shown that self-consistent charge distributions can be approximated by the superposition of the neutral atomic charges, at least in order to obtain binding energies.[44] This point justifies the omission of the interatomic electrostatic interactions in the usual method. However, this point also indicates that unrealistic large charge transfers appearing frequently in tight-binding calculations should be suppressed by a proper scheme, such as the present method or the local charge neutrality condition.[45] The latter corresponds to the usage of an infinite large value of $U$.

It should be noted that the effects of the intra-atomic electrostatic interactions are not so large quantitatively in the total-energy increases of the present boundaries. It has been found that the local charge neutrality condition generally gives the largest values for the total energy increases, and that the scheme without any conditions gives the smallest values with respect to the same atomic configurations. The differences between these values do not exceed several percent of the total energy increases in the present case of the $\langle 011 \rangle$ $\Sigma = 3$ twist boundaries, for example.

TABLE I. The parameter values in the transferable SETB method for Si (Ref. 35). $\Delta E_{\rm sp^3} = 4.39$ eV, $\lambda_1 = 1.086$ Å$^{-2}$, $\lambda_2 = 8.511$ Å$^{-1}$, $b_0 = 300.2715$ eV Å$^5$, and $b_1 = 4.8227$ eV Å$^5$.

| | Hopping integrals | | | | |
|---|---|---|---|---|---|
| | $ss\sigma$ | $sp\sigma$ | $pp\sigma$ | $pp\pi$ | Repulsive potential |
| $\nu$ | 4 | 3 | 2 | 2 | 5 |
| $\eta$ (eV Å$^{\nu}$) | −63.9 | 27.7 | 13.1 | −2.94 | |
| $\mu$ (Å$^{-1}$) | 5.96 | 5.96 | 2.55 | 2.55 | 2.55 |
| $R_c$ (Å) | 3.17 | 3.17 | 3.83 | 3.83 | 3.83 |

### C. Lattice relaxation

All calculations of boundaries are carried out by use of the supercell technique. The periodicity normal to the interface is imposed by alternately stacking symmetric boundary planes in addition to the two-dimensional periodicity parallel to the interface of the CSL boundary. Thus the conventional technique of band calculation can be applied to the supercell with a large unit cell containing two interfaces.

For integration over the Brillouin zone, special-**k** points[46] are used. The density of the **k** points is large enough. The lowest density of the **k** points used in the supercell calculations is equal to that corresponding to 20 special-**k** points in the irreducible part of the Brillouin zone of diamond Si. In order to avoid the problems of degenerated states at the Fermi level, the occupancies of the uppermost states are distributed among all the degenerated states.

In lattice relaxations, the atomic positions are relaxed according to the atomic forces, although the atoms in the central one or two atomic layers in the bulk regions between the interfaces in the supercells are fixed. In each step of the relaxations, the atomic forces are obtained after the self-consistent iteration, which is terminated if differences between input and output occupancies of the

respective atoms are all kept within a given tolerance. It is $10^{-3}$ electrons for small cells, and $10^{-4}$ electrons for large cells. The two types of cells are explained in Sec. III. The relaxation is terminated if the atomic forces are all smaller than 0.1 eV/Å.

In relaxed configurations, the coordination defects are analyzed by the coordination radius of 2.8 Å. Of course, the radius cannot be defined absolutely. Values from 2.7 to 2.9 Å are used in studies of amorphous Si,[47–49] which were determined by the first minima in the pair distribution functions of the calculated configurations of amorphous Si. Such a small dispersion should not change the results of the analyses so much, although this might give rise to several mutual transformations between three-coordinated and five-coordinated defects.

## III. MODELS OF BOUNDARIES AND RIGID-BODY TRANSLATIONS

### A. Models and supercell configurations

The twist boundaries in the present study are constructed by two ideal surfaces of two semicrystals, which are formed by cutting the bulk crystal into two. Thus the present boundaries contain no interstitials or vacancies. The ⟨111⟩ $\Sigma=7$ twist boundary is formed by rotating ideal (111) surfaces around the ⟨111⟩ axis. The two types of rotation angles, 38.2° and 98.2°, generate different boundaries, although the size of the CSL unit cell is identical. The ⟨011⟩ $\Sigma=3$ twist boundary is formed by rotating ideal (011) surfaces around the ⟨011⟩ axis. The boundaries with the two types rotation angles, 70.5° and 109.5°, can be transformed into each other by introducing rigid-body translations parallel to the interface. Thus the present study deals only with the boundary with the rotation angle 109.5°. The ⟨001⟩ $\Sigma=5$ twist boundary is formed by rotating ideal (001) surfaces around the ⟨001⟩ axis. The two types of rotation angles, 36.9° and 53.1°, generate different boundaries, although the size of the CSL unit cell is identical.

Figures 1–3 show configurations of respective twist boundaries before lattice relaxations and without any rigid-body translations. In these figures, the CSL unit cells are indicated by dashed lines, and the CSL vectors $\mathbf{R}_1$ and $\mathbf{R}_2$ are expressed by using the coordinate axes of the lower crystals. In the present study, the rigid-body translations parallel to the interface are defined as shifts of the upper crystals from the configurations shown in Figs. 1–3, and can be expressed by fractions of the vectors $\mathbf{R}_1$ and $\mathbf{R}_2$. The translations normal to the interface are defined as compared with the ideal distances between the planes in the bulk crystal. It should be noted that the configurations in Fig. 3 are similar to those used in the previous calculations of Ge (Ref. 32) for comparison.

We have used the following supercells for the relaxations against various rigid-body translations. The supercells of the ⟨111⟩ $\Sigma=7$ twist boundary contain 84 atoms, where the interfaces are repeated between six (111) atomic layers. The distance between the interfaces is about 9.4 Å. The supercells of the ⟨011⟩ $\Sigma=3$ twist boundary contain 60 atoms, where the interfaces are repeated be-

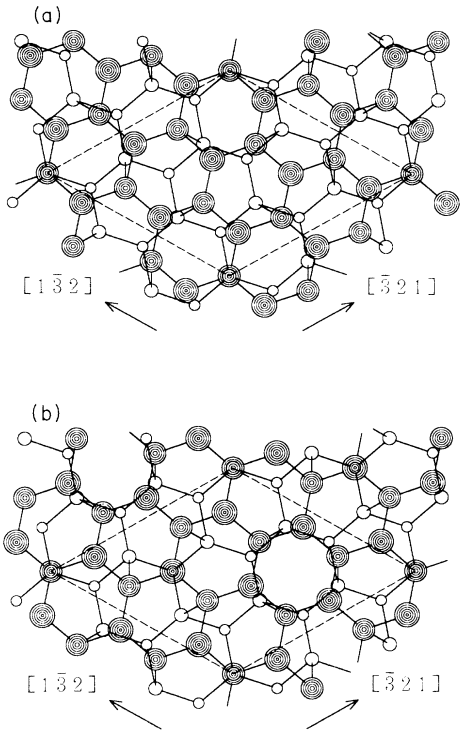


FIG. 1. Unrelaxed atomic configurations without translations for the ⟨111⟩ $\Sigma=7$ twist boundaries in Si. (a) The $\Sigma=7$ boundary with a rotation angle of 38.2°. (b) The $\Sigma=7$ boundary with a rotation angle of 98.2°. Two upper and two lower atomic layers are projected along the ⟨111⟩ axis. Rigid-body translations are defined as shifts of the upper crystals as compared with these configurations. The CSL unit cells are defined by $\mathbf{R}_1=a_0[-3,2,1]/2$ and $\mathbf{R}_2=a_0[1,-3,2]/2$ as indicated by broken lines.

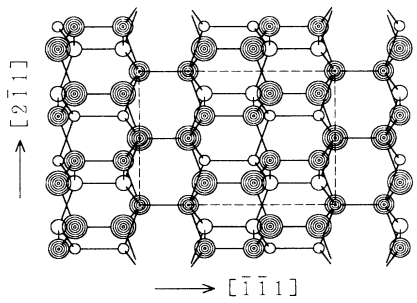


FIG. 2. Unrelaxed atomic configuration without translations for the ⟨011⟩ $\Sigma=3$ twist boundary in Si with a rotation angle of 109.5°. Two upper and two lower atomic layers are projected along the ⟨011⟩ axis. Rigid-body translations are defined as shifts of the upper crystal as compared with this configuration. The CSL unit cell is defined by $\mathbf{R}_1=a_0[-1,-1,1]$ and $\mathbf{R}_2=a_0[2,-1,1]/2$ as indicated by broken lines.

tween five (011) atomic layers. The distance between the interfaces is about 9.6 Å. The supercells of the ⟨001⟩ $\Sigma=5$ twist boundary contain 60 atoms, where the interfaces are repeated between six (001) atomic layers. The distance between the interfaces is about 8.1 Å. In the relaxations, the atoms in the two central (111) layers, those in the one central (011) layer, and those in the two central (001) layers in the bulk regions are fixed at initial positions.

In order to obtain more quantitative results and to search for the most stable configurations, we perform additional relaxations of larger supercells with respect to selected rigid-body translations which give relatively stable configurations. The large supercells of the ⟨111⟩ $\Sigma=7$ boundary contain 168 atoms, where the interfaces are repeated between 12 (111) layers, and the distance between the interfaces is about 18.8 Å. Those of the ⟨011⟩ $\Sigma=3$ boundary contain 156 atoms, where the interfaces are repeated between 13 (011) layers, and the distance between the interfaces is about 25.0 Å. Those of the ⟨001⟩ $\Sigma=5$ boundary contain 140 atoms, where the interfaces are repeated between 14 (001) layers, and the distance between the interfaces is about 19.5 Å.

### B. Rigid-body translations and DSC unit cells

Rigid-body translations are introduced between the two bulk crystals before the relaxations. The symmetric properties and periodicity of the initial configurations are naturally preserved in the relaxations. In such cases, the meaningful translations parallel to the interface are limited within the irreducible part of the unit cell of the DSC (displacement shift complete) lattice,[3] as discussed in Ref. 32.

The DSC unit cells in the boundary planes of the $\Sigma=7$, $\Sigma=3$, and $\Sigma=5$ boundaries are defined by $\mathbf{R}_1/7$ and $\mathbf{R}_2/7$, $\mathbf{R}_1/3$ and $\mathbf{R}_2/3$, and $\mathbf{R}_1/5$ and $\mathbf{R}_2/5$, respectively, and are $\frac{1}{49}$, $\frac{1}{9}$, and $\frac{1}{25}$ of the CSL unit cells, respectively. Figures 4–6 show the irreducible parts of the DSC unit cells of the present twist boundaries. The irreducible part means that a translation parallel to the interface outside the irreducible part leads to a configuration equivalent to that with a translation in the irreducible part by the symmetric property. These irreducible parts have been found by iterating relaxations of the present supercells with various translations parallel to the interface by using the Stillinger-Weber potential to save computing time. The irreducible parts of the $\Sigma=5$ boundaries are identical to those in Ref. 32.

In order to examine the overall features of the energies and atomic structures of the present twist boundaries, we have dealt with translations of the mesh points in the irreducible parts of the DSC unit cells indicated by double

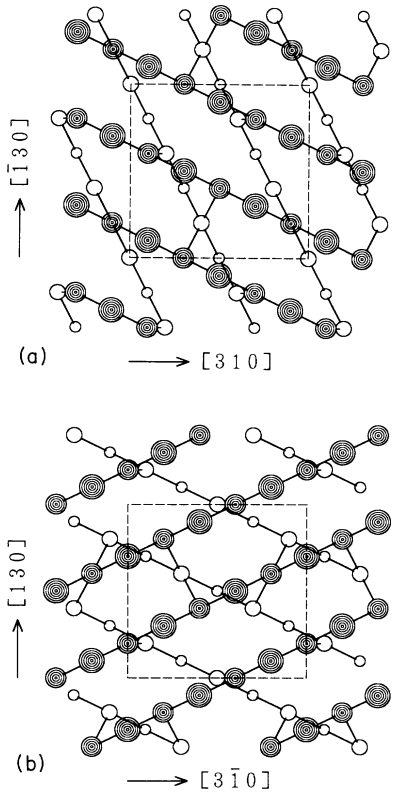


FIG. 3. Unrelaxed atomic configurations without translations for the ⟨001⟩ $\Sigma=5$ twist boundaries in Si. (a) The $\Sigma=5$ boundary with a rotation angle of 36.9°. (b) The $\Sigma=5$ boundary with a rotation angle of 53.1°. Two upper and two lower atomic layers are projected along the ⟨001⟩ axis. Rigid-body translations are defined as shifts of the upper crystals as compared with these configurations. The CSL unit cells are defined by $\mathbf{R}_1=a_0[3,1,0]/2$ and $\mathbf{R}_2=a_0[-1,3,0]/2$ or by $\mathbf{R}_1=a_0[3,-1,0]/2$ and $\mathbf{R}_2=a_0[1,3,0]/2$ as indicated by broken lines.

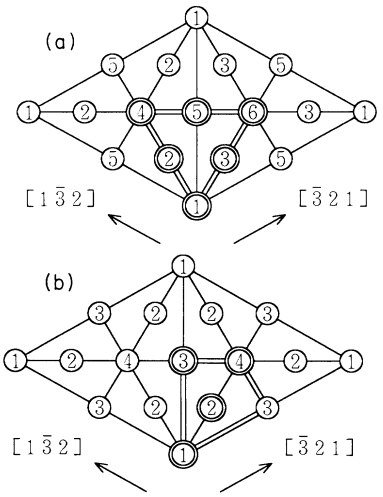


FIG. 4. DSC unit cells and the irreducible parts for (a) the ⟨111⟩ $\Sigma=7$ twist boundary in Si with a rotation angle of 38.2°, and (b) that with a rotation angle of 98.2°. The DSC unit cells are defined by $\mathbf{R}_1/7$ and $\mathbf{R}_2/7$. The irreducible parts are enclosed by double lines. The circles are the mesh points, and the numbers indicate equivalent translations generating configurations that are equivalent to one another. The double circles are the mesh points in the irreducible parts dealt with in the present calculations. The numbers in the double circles have the same meaning as the Trans. No. column in Table II.

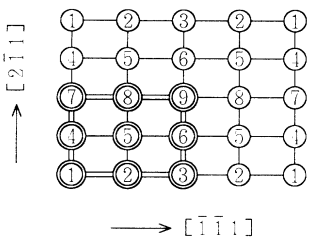


FIG. 5. DSC unit cell and the irreducible part for the ⟨011⟩ $\Sigma=3$ twist boundary in Si with a rotation angle of 109.5°. The DSC unit cell is defined by $\mathbf{R}_1/3$ and $\mathbf{R}_2/3$. The irreducible part is enclosed by double lines. The circles are the mesh points, and the numbers indicate equivalent translations generating configurations that are equivalent to one another. The double circles are the mesh points in the irreducible part dealt with in the present calculations. The numbers in the double circles have the same meaning as the Trans. No. column in Table III.

circles in Figs. 4–6. The distances between the neighboring mesh points are 0.42 Å for the $\Sigma=7$ boundary, 0.78 and 0.55 Å for the $\Sigma=3$ boundary, and 0.43 Å for the $\Sigma=5$ boundary.

Concerning the translations normal to the interface, we have employed those optimized in the 0.1-Å grid by lattice relaxations using the Stillinger-Weber potential for respective translations parallel to the interface to save computing time. Of course, it is more desirable to optimize the translations normal to the interface by using the transferable SETB method. For relaxations of large supercells with respect to several translations parallel to the interface, the translations normal to the interface have been optimized by iterating the relaxations of the small supercells by using the transferable SETB method.

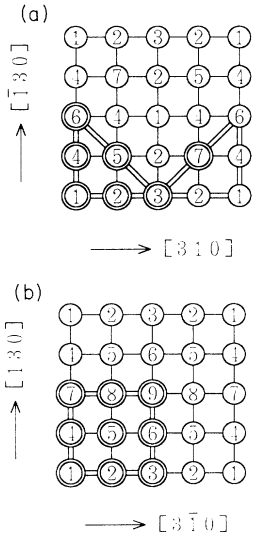


FIG. 6. DSC unit cells and the irreducible parts for (a) the ⟨001⟩ $\Sigma=5$ twist boundary in Si with a rotation angle of 36.9°, and (b) that with a rotation angle of 53.1°. The DSC unit cells are defined by $\mathbf{R}_1/5$ and $\mathbf{R}_2/5$. The irreducible parts are enclosed by double lines. The circles are the mesh points, and the numbers indicate equivalent translations generating configurations that are equivalent to one another. The double circles are the mesh points in the irreducible parts dealt with in the present calculations. The numbers in the double circles have the same meaning as the Trans. No. column in Table IV.

## IV. ENERGIES AND ATOMIC CONFIGURATIONS

### A. The {122} $\Sigma=9$ tilt boundary

First, in order to examine the validity of the present scheme, and in order to clarify the features of the tilt boundaries, we have performed the relaxation of the {122} $\Sigma=9$ tilt boundary as a typical CSL tilt boundary frequently observed in polycrystalline Si. This boundary is constructed by rotating the two crystals around the ⟨011⟩ axis by 38.9°, and the boundary plane {122} is parallel to the rotation axis. The CSL unit cell in the boundary plane is expressed by $\mathbf{R}_1=a_0[4,1,-1]/2$ and $\mathbf{R}_2=a_0[011]/2$. We deal with an atomic model containing a glide-plane symmetry and consisting of a zigzag arrangement of five- and seven-membered rings without any coordination defects. This configuration has been observed by HRTEM,[7,9,10,12] and has been dealt with theoretically.[15,19,20]

The supercell and the **k** points are the same as those used in Ref. 19. The supercell contains 144 atoms, where the distance between the interfaces is about 32.6 Å. Only the translation normal to the interface is permitted by the symmetric property, and has been optimized by relaxations of the supercell of 80 atoms by using the transferable SETB method.

The optimized translation is +0.06 Å. The calculated interfacial energy $E_{gb}$ is 0.32 J/m$^2$. The energy per boundary atom is 0.11 eV. The relaxed configuration is stable with small bond-length and bond-angle distortions ranging from −1.6 to +1.5%, and from −16.2° to +20.8°, respectively. No electronic states exist inside the minimum band gap.

The present results are in good agreement with previous calculations of this boundary using band-structure calculations,[15,19,20] and this shows the validity of the present scheme. For example, $E_{gb}$ are 0.32, 0.29, and 0.34 J/m$^2$ by the SETB method,[15] by the *ab initio* pseudopotential method,[20] and by the self-consistent tight-binding method,[19] respectively. The absolute values of the bond-length deviations do not exceed 1.5%,[20] and the bond-length and bond-angle deviations range from −1.9 to +1.5% and from −16.0° to +19.9°, respectively.[19] No states exist inside the minimum band gap.

It should be noted that these features are common to all previous results for symmetrical tilt boundaries in Si or Ge based on band-structure calculations, including the {211} $\Sigma=3$ boundary in Si,[16,18] and the ⟨001⟩ tilt boundaries in Si (Refs. 16, 17, and 21) and Ge.[22] In such calculations, $E_{gb}$ ranges from 0.26 to 0.46 J/m$^2$ in Si. The maximum absolute values of bond-length and bond-angle deviations are within several percent and within about 20°, respectively, which cause no states inside the

minimum band gap, although localized states are frequently generated at the band edges. In the present study, the results for twist boundaries are compared with these features of the tilt boundaries in Si or Ge.

### B. The ⟨111⟩ Σ=7 twist boundary

The calculated interfacial energies of the 84-atom cells of the Σ=7 boundaries with the rotation angles 38.2° and 98.2° are listed in Table II. In Table II, $E_F$ and the numbers of the coordination defects or the maximum bond distortions are also listed. $E_F$ is the uppermost occupied level from the bulk valence-band maximum, which gives information about the occupied gap states.

In these two boundaries, $E_{gb}$ ranges from 1.3 to 1.7 J/m$^2$. Several configurations with three-coordinated defects contain larger energies and deep states in the band gap, although some configurations with no coordination defects also contain large energies and deep states. The configurations with no translation parallel to the interface, namely those of Trans. 1, are the most stable in both the boundaries, and contain no coordination defects. However, these configurations have much larger interfacial energies than the tilt boundaries, and contain shallow states in the band gap as indicated by the values of $E_F$. This is because the maximum values and densities of the bond distortions are larger than those of the tilt boundaries.

The relaxed configurations of the 84-atom cells are shown in Figs. 7 and 8. In both the boundaries, the most stable configurations of Trans. 1 contain seven interfacial bonds in the CSL unit cell. Within these seven interfacial bonds, one type of bond at the coincidence sites, namely at the corners of the CSL unit cells shown in Figs. 7 and 8, has very small bond distortions because this bond is parallel to the rotation axis. The other six interfacial bonds in the unit cell have larger bond distortions.

Concerning the boundary of 38.2° shown in Fig. 7, the bonding network of the configuration of Trans. 3 is similar to that of Trans. 1. In the configuration of Trans. 2, as compared with that of Trans. 1, two interfacial bonds in the CSL unit cell are broken, one new bond is formed, and two dangling bonds remain. The bonding networks of the configurations of Trans. 4 and Trans. 5 are similar to that of Trans. 2. In the configuration of Trans. 6 as compared with that of Trans. 3, two interfacial bonds in the CSL unit cell are broken, one new bond is formed, and two dangling bonds remain.

About the boundary of 98.2° shown in Fig. 8, the bonding network of the configuration of Trans. 2 is similar to that of Trans. 1. The configuration of Trans. 3 is formed by switching three interfacial bonds in the CSL unit cell of the configuration of Trans. 2. In the configuration of Trans. 4 as compared with that of Trans. 2, two interfacial bonds in the CSL unit cell are broken, one new bond is formed, and two dangling bonds remain.

In both the boundaries, the changes of the configurations from those of Trans. 1 by the translations parallel to the interface can be explained as follows. When the translations parallel to the interface are small, the bonding network is not changed, although the energies and bond distortions are increased. Large translations cause the switching of the interfacial bonds, and sometimes result in the generation of three-coordinated defects.

The configurations of Trans. 1 are the most stable for both boundaries. However, the energy minima at Trans. 1 against the rigid-body translations do not seem to be so sharp or deep for both the boundaries. In order to examine this point more quantitatively, we have performed re-

TABLE II. Energies and structural disorder of the ⟨111⟩ Σ=7 twist boundaries in Si against the rigid-body translations calculated by using 84-atom cells. The translations parallel to the interface are expressed by fractions of the CSL vectors. $T_z$ is the translation normal to the interface used in the calculations, which is optimized by the Stillinger-Weber potential. $E_{gb}$ is the interfacial energy. $E_F$ is the highest occupied level from the bulk valence-band maximum. In the column for structural disorder, the numbers of three-coordinated [dangling bond (DB)] or five-coordinated defects [floating bond (FB)] in the CSL unit cell are listed. In cases with no coordination defects, maximum bond-length and bond-angle deviations are listed.

| Trans. No. | Translation ($\times\mathbf{R}_1$, $\times\mathbf{R}_2$) | $T_z$ (Å) | $E_{gb}$ (J/m$^2$) | $E_F$ (eV) | Structural disorder |
|---|---|---|---|---|---|
| | | Σ=7 boundary of 38.2° | | | |
| Trans. 1 | (0.0, 0.0) | −0.1 | 1.31 | 0.20 | +4.5%, −24.0° |
| Trans. 2 | ($\frac{1}{42}$, $\frac{1}{21}$) | −0.1 | 1.38 | 0.66 | DB:2 |
| Trans. 3 | ($\frac{1}{21}$, $\frac{1}{42}$) | −0.1 | 1.38 | 0.27 | +5.9%, −27.1° |
| Trans. 4 | ($\frac{1}{21}$, $\frac{2}{21}$) | −0.1 | 1.33 | 0.65 | DB:2 |
| Trans. 5 | ($\frac{1}{14}$, $\frac{1}{14}$) | −0.1 | 1.38 | 0.65 | DB:2 |
| Trans. 6 | ($\frac{2}{21}$, $\frac{1}{21}$) | −0.1 | 1.69 | 1.15 | DB:2 |
| | | Σ=7 boundary of 98.2° | | | |
| Trans. 1 | (0.0, 0.0) | −0.1 | 1.32 | 0.41 | +4.6%, −25.1° |
| Trans. 2 | ($\frac{1}{21}$, $\frac{1}{42}$) | −0.1 | 1.39 | 0.59 | +6.6%, −28.9° |
| Trans. 3 | ($\frac{1}{14}$, $\frac{1}{14}$) | −0.1 | 1.51 | 0.45 | +6.5%, −28.7° |
| Trans. 4 | ($\frac{2}{21}$, $\frac{1}{21}$) | −0.1 | 1.50 | 1.02 | DB:2 |

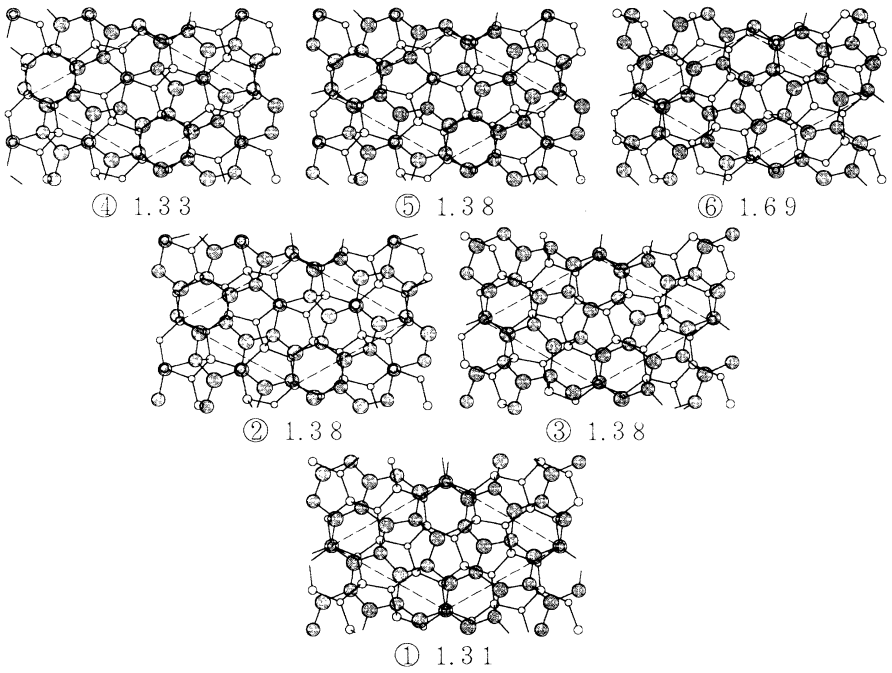


FIG. 7. Relaxed atomic configurations of the ⟨111⟩ $\Sigma=7$ twist boundary in Si with a rotation angle of 38.2°, against the rigid-body translations. The atomic configurations for the six translations in the irreducible part of the DSC unit cell are shown by the same arrangement as the translations in Fig. 4(a). Interfacial energies of respective configurations are also shown in units of J/m$^2$.

laxations of the 168-atom cells of the boundaries of 38.2° and of 98.2° with Trans. 1 and the optimized translations normal to the interface, +0.10 Å and zero, respectively. The configurations and energies obtained are not so different from those of the small cells shown in Figs. 7 and 8. $E_{gb}$ of the boundary of 38.2° is 1.28 J/m$^2$, and that of 98.2° is also 1.28 J/m$^2$, although the latter is a little larger. The energy per boundary atom is 0.51 eV for both the boundaries. The bond-length and bond-angle distortions of the boundary of 38.2° range from −1.4 to +4.6% and from −23.5° to +21.3°, respectively, and those of the boundary of 98.2° range from −1.4% to +4.9% and −25.0° to +22.1°.

It is clear that the energy minima at Trans. 1 in both boundaries are not so deep. The relaxed configurations of Trans. 1 contain larger absolute values and densities of bond distortions and larger interfacial energies than those of the tilt boundaries. In particular, large bond stretchings exist at the interfacial bonds and the neighboring back bonds, except for the bonds at the coincidence sites.

These bond distortions of Trans. 1 generate shallow states at the band edges. In these configurations of Trans. 1, all the valence-band-edge states are occupied, and $E_F$ indicates the uppermost valence-band-edge state. It has been found that the value of $E_F$ become gradually smaller through the relaxation procedure, and the values of $E_F$ for the 184-atom cells are smaller than those for the 84-atom cells because of relatively small degrees of bond distortions. The $E_F$ of the 98.2° boundary for the 184-atom cell is 0.18 eV. The $E_F$ of the 38.2° boundary for the 184-atom cell is 0.05 eV because of only a few shallow states at the valence-band edge. However, in this boundary, there remain empty shallow states at the conduction-band edge.

Generally, the configurations of the ⟨111⟩ $\Sigma=7$ twist boundaries are not so complicated compared with the other twist boundaries described in the following subsections. It seems that the features of energies and configurations against the translations obtained by the small cells are valid enough, although the translations normal to the interface are not strictly optimized. This simplicity can be explained by the morphology of the ideal (111) surfaces, where respective surface atoms have

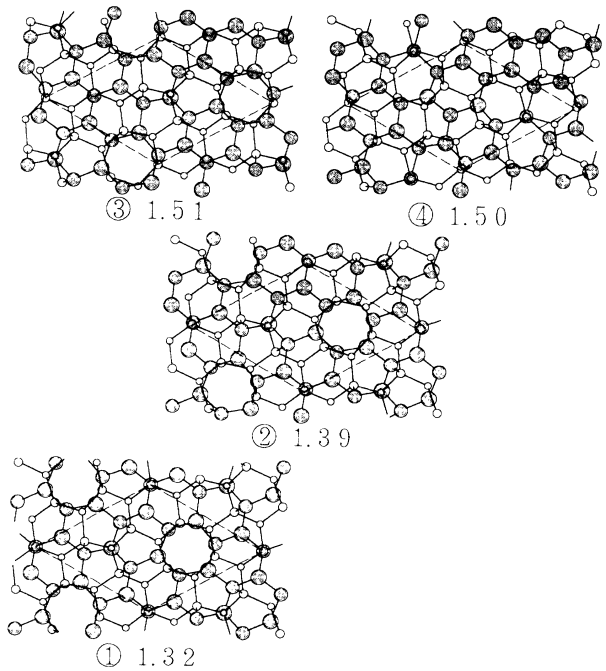


FIG. 8. Relaxed atomic configurations of the ⟨111⟩ $\Sigma=7$ twist boundary in Si with a rotation angle of 98.2°, against the rigid-body translations. The atomic configurations for the four translations in the irreducible part of the DSC unit cell are shown by the same arrangement as the translations in Fig. 4(b). Interfacial energies of respective configurations are also shown in units of J/m$^2$.

only one dangling bond pointing to the direction normal the surface. It is possible to construct configurations of interfaces without any coordination defects for proper translations, by creating interfacial bonds with such dangling bonds facing each other at the interface. However, large bond distortions, especially bond stretchings, are inevitably introduced, except at the sites of good coincidence, because the configurations of ideal (111) surfaces do not have enough of a degree of freedom for relaxation.

### C. The ⟨011⟩ $\Sigma=3$ twist boundary

The calculated interfacial energies of the 60-atom cells of the $\Sigma=3$ boundary with the rotation angle 109.5° are listed in Table III. $E_{gb}$ ranges from 1.1 to 3.1 J/m$^2$. The configurations with no coordination defects and relatively small bond distortions have relatively small energies, and the most stable configuration is that of Trans. 1. However, this configuration also has a much larger interfacial energy than that of the tilt boundaries, and contains shallow states in the band gap, because of the large density and absolute values of bond distortions.

The relaxed configurations of the 60-atom cells are shown in Fig. 9. The bonding network of the configuration of Trans. 2 is similar to that of Trans. 1. The bonding networks of the configurations of Trans. 5 and Trans. 8 are similar to that of Trans. 7. In the configurations of these two groups of the same bonding networks, there exist six interfacial bonds without any coordination defects, and two four-membered rings with large bond distortions in the CSL unit cell, respectively. In these two groups of configurations, the configurations of Trans. 1 and Trans. 7 are the most stable, respectively. It can be said that there exist two shallow energy minima at Trans. 1 and Trans. 7 against the rigid-body translations, although the configurations at these energy minima still contain larger bond distortions and energies than those of the tilt boundaries.

In the configurations between these energy minima, larger bond distortions or five-coordinated defects are introduced, or very complex structures are generated. The main difference between the configurations of Trans. 1 and Trans. 7 is the bonding network at one of the three atomic chains along the [2,−1,1] direction in the CSL unit cell. The configuration of Trans. 4 between these two configurations contains the intermediate structure with five-coordinated defects at this atomic chain. The configurations with large translations along the [−1,−1,1] direction such as those of Trans. 3, Trans. 6, and Trans. 9 are very complex, and contain very large interfacial energies with five-coordinated defects or large bond distortions. In these configurations, several bonds along the (011) surfaces are broken, and are used to form interfacial bonds.

In order to examine the energy minimum at Trans. 1, we have performed the relaxation of the 156-atom cell of this boundary with Trans. 1 and the optimized translation normal to the interface, +0.10 Å. However, the configuration and energy obtained are not so different from those of the 60-atom cell shown in Fig. 9. $E_{gb}$ is 1.02 J/m$^2$, and the energy per boundary atom is 0.33 eV. The bond-length and bond-angle distortions range from −2.4 to +2.0% and from −35.5° to +28.5°, respectively. In particular, there exist large bond-angle distortions associated with the two four-membered rings in the unit cell. All the valence-band-edge states are occupied, and $E_F$ is 0.16 eV, which is the same as the value of the 60-atom cell.

It can be said that this energy minimum at Trans. 1 is not so deep. This configuration contains larger absolute values and density of bond distortions, and a larger interfacial energy than those of the tilt boundaries. This configuration contains the shallow states at the valence-band and conduction-band edges inside the minimum band gap because of the bond distortions.

We have also performed a relaxation of the 156-atom cell of this boundary with Trans. 4 and the optimized translation normal to the interface, +0.10 Å. The

TABLE III. Energies and structural disorder of the ⟨011⟩ $\Sigma=3$ twist boundary in Si against the rigid-body translations calculated by using 60-atom cells. The translations parallel to the interface are expressed by fractions of the CSL vectors. $T_z$ is the translation normal to the interface used in the calculations, which is optimized by the Stillinger-Weber potential. $E_{gb}$ is the interfacial energy. $E_F$ is the highest occupied level from the bulk valence-band maximum. In the column for structural disorder, the numbers of three-coordinated [dangling bond (DB)] or five-coordinated defects [floating bond (FB)] in the CSL unit cell are listed. In cases with no coordination defects, maximum bond-length and bond-angle deviations are listed.

| Trans. No. | Translation ($\times\mathbf{R}_1$, $\times\mathbf{R}_2$) | $T_z$ (Å) | $E_{gb}$ (J/m$^2$) | $E_F$ (eV) | Structural disorder |
|---|---|---|---|---|---|
| Trans. 1 | (0.0, 0.0) | +0.4 | 1.13 | 0.16 | +3.1%, −35.8° |
| Trans. 2 | ($\frac{1}{12}$, 0.0) | +0.4 | 1.33 | 0.18 | +4.0%, −35.9° |
| Trans. 3 | ($\frac{1}{6}$, 0.0) | +0.3 | 2.69 | 1.33 | +4.9%, +40.1° |
| Trans. 4 | (0.0, $\frac{1}{12}$) | +0.3 | 1.21 | 0.47 | FB:2 |
| Trans. 5 | ($\frac{1}{12}$, $\frac{1}{12}$) | +0.1 | 1.46 | 0.53 | +9.1%, −30.6° |
| Trans. 6 | ($\frac{1}{6}$, $\frac{1}{12}$) | −0.2 | 1.73 | 0.29 | +7.4%, +24.6° |
| Trans. 7 | (0.0, $\frac{1}{6}$) | +0.3 | 1.19 | 0.16 | +6.7%, −26.1° |
| Trans. 8 | ($\frac{1}{12}$, $\frac{1}{6}$) | +0.3 | 1.38 | 0.27 | +6.9%,−27.1° |
| Trans. 9 | ($\frac{1}{6}$, $\frac{1}{6}$) | −0.1 | 3.05 | 1.41 | FB:12 |

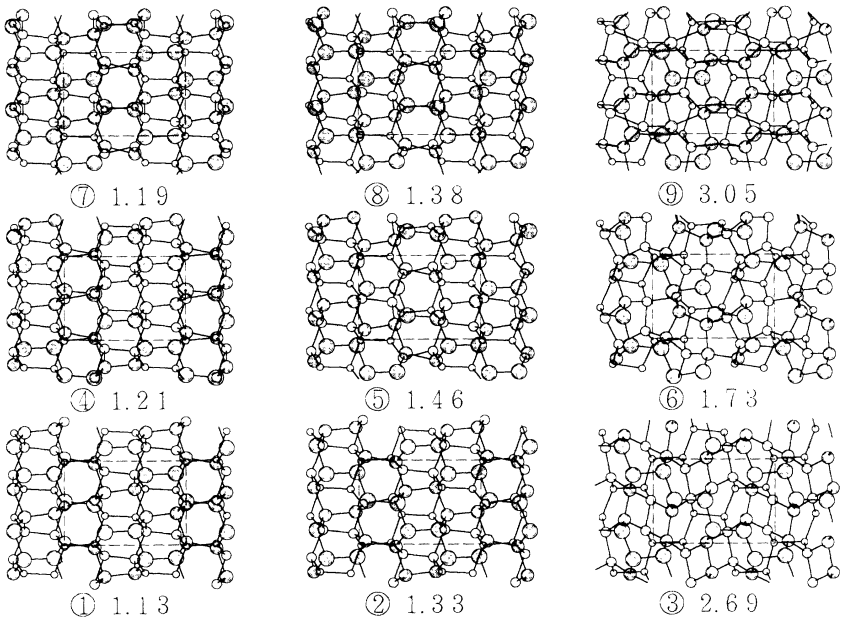


FIG. 9. Relaxed atomic configurations of the ⟨011⟩ $\Sigma=3$ twist boundary in Si with a rotation angle of 109.5°, against the rigid-body translations. The atomic configurations for the nine translations in the irreducible part of the DSC unit cell are shown by the same arrangement as the translations in Fig. 5. Interfacial energies of respective configurations are also shown in units of J/m$^2$.

configuration obtained has a bonding network similar to that of Trans. 7. Thus the configuration of Trans. 4 with five-coordinated defects by the 60-atom cell shown in Fig. 9 seems to be only quasistable. However, the interfacial energy is almost the same as that of the 60-atom cell (1.21 J/m$^2$), and bond distortions as large as +8.1% and −28.9° are contained.

Generally, the configurations of the ⟨011⟩ $\Sigma=3$ twist boundary are not so complicated compared with the ⟨001⟩ $\Sigma=5$ twist boundaries described in Sec. IV D. It seems that the features of energies and configurations against the translations obtained by the small cells are valid enough, although the translations normal to the interface are not strictly optimized. For translations such as Trans. 1 and Trans. 7, where the atomic rows along the $[2,-1,1]$ direction of the two (011) surfaces coincide with each other at the interface, relatively stable configurations without any coordination defects can be constructed. This is also related to the morphology of the ideal (011) surface, where respective surface atoms have only one dangling bond, as well as to the ideal (111) surface. However, surface atoms are connected to each other by the bond along the surface, and dangling bonds of neighboring surface atoms have different directions. Thus configurations of interfaces frequently contain four-membered rings with large bond-angle distortions.

### D. The ⟨001⟩ $\Sigma=5$ twist boundary

The calculated interfacial energies of the 60-atom cells of the $\Sigma=5$ boundaries with the rotation angles 36.9° and 53.1° are listed in Table IV. $E_{gb}$ ranges from 2.2 to 2.9 J/m$^2$ for the boundary of 36.9°, and from 2.5 to 3.0 J/m$^2$ for the boundary of 53.1°. It seems that the configurations for the boundary of 36.9° have slightly smaller energies than those for the boundary of 53.1°. However, the interfacial energies for both boundaries are very large compared with the ⟨111⟩ $\Sigma=7$ and ⟨011⟩ $\Sigma=3$ boundaries. Three- or five-coordinated defects are frequently contained, and there exists a configuration with two-coordinated defects. Configurations with no coordination defects have very large bond distortions such as bond-angle distortions over +50°. All the configurations contain deep states in the band gap.

The relaxed configurations of the 60-atom cells are shown in Figs. 10 and 11. The configurations are very complex as compared with the other twist boundaries. All the configurations for the boundary of 36.1° shown in Fig. 10 have different bonding networks. The differences between the bonding networks of the configurations with neighboring translations in Fig. 10 can be explained by bond switching among the interfacial bonds and dimer bonds along the surfaces.[32] For example, the configuration of Trans. 1 is generated from that of Trans. 4 by breaking one interfacial bond and one dimer bond at the five-coordinated defect, and by forming one new interfacial bond in the CSL unit cell. Thus two three-coordinated defects and only one dimer bond exist in the CSL unit cell of Trans. 1. The configuration of Trans. 2 is generated from that of Trans. 1 by breaking two interfacial bonds, and by forming one dimer bond and one interfacial bond in the CSL unit cell. Thus the position of one three-coordinated defect is changed. The configuration of Trans. 5 is formed from that of Trans. 2 by breaking one dimer bond, and by forming one dimer bond and one interfacial bond, which eliminates the three-coordinated defects in the CSL unit cell.

About the configurations of the boundary of 53.1° shown in Fig. 11, the bonding networks of the configurations of Trans. 7 and Trans. 8 are similar to that of Trans. 4, where four dimer bonds and four five-coordinated defects exist in the CSL unit cell. The other configurations have different bonding networks. The differences between the bonding networks of the configurations with neighboring translations in Fig. 11 can also be explained by the bond switching among the

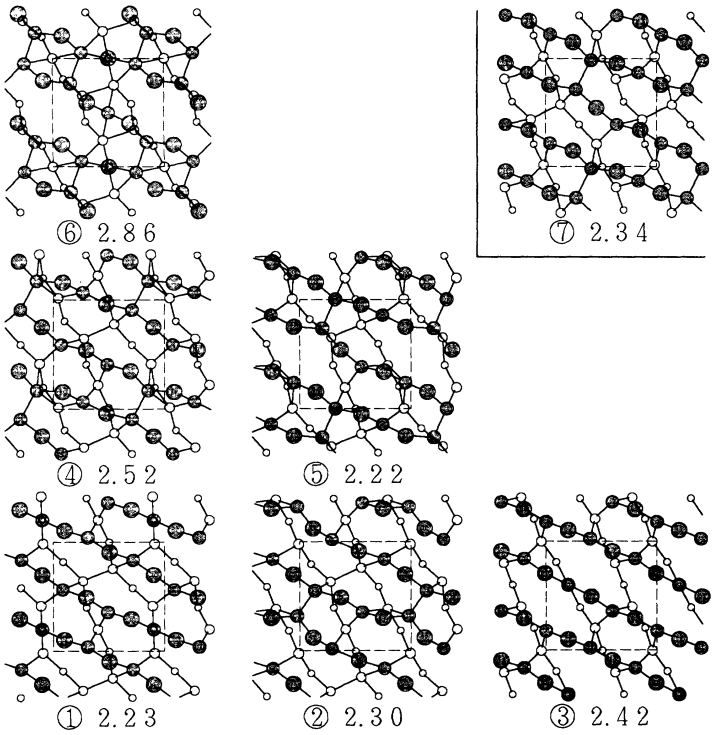


FIG. 10. Relaxed atomic configurations of the ⟨001⟩ $\Sigma=5$ twist boundary in Si with a rotation angle of 36.9°, against the rigid-body translations. The atomic configurations for the seven translations in the irreducible part of the DSC unit cell are shown by the same arrangements as the translations in Fig. 6(a), with the exception of the enclosed structure of Trans. 7. Interfacial energies of respective configurations are also shown in units of $J/m^2$.

TABLE IV. Energies and structural disorder of the ⟨001⟩ $\Sigma=5$ twist boundaries in Si against the rigid-body translations calculated by using 60-atom cells. The translations parallel to the interface are expressed by fractions of the CSL vectors. $T_z$ is the translation normal to the interface used in the calculations, which is optimized by the Stillinger-Weber potential. $E_{gb}$ is the interfacial energy. $E_F$ is the highest occupied level from the bulk valence-band maximum. In the column for structural disorder, the numbers of three-coordinated [dangling bond (DB)] or five-coordinated defects [floating bond (FB)] in the CSL unit cell are listed. TD also indicates the number of two-coordinated defects in the CSL unit cell. In cases with no coordination defects, maximum bond-length and bond-angle deviations are listed.

| Trans. No. | Translation ($\times\mathbf{R}_1$, $\times\mathbf{R}_2$) | $T_z$ (Å) | $E_{gb}$ ($J/m^2$) | $E_F$ (eV) | Structural disorder |
|---|---|---|---|---|---|
| | | $\Sigma=5$ boundary of 36.9° | | | |
| Trans. 1 | (0.0, 0.0) | +0.1 | 2.23 | 0.71 | DB:2 |
| Trans. 2 | ($\frac{1}{20}$, 0.0) | +0.1 | 2.30 | 0.60 | DB:2 |
| Trans. 3 | ($\frac{1}{10}$, 0.0) | +0.4 | 2.42 | 1.17 | DB:6 |
| Trans. 4 | (0.0, $\frac{1}{20}$) | +0.1 | 2.52 | 1.17 | DB:1, FB:1 |
| Trans. 5 | ($\frac{1}{20}$, $\frac{1}{20}$) | +0.1 | 2.22 | 0.60 | +6.6%, +53.0° |
| Trans. 6 | (0.0, $\frac{1}{10}$) | +0.3 | 2.86 | 0.93 | FB:4 |
| Trans. 7 | ($\frac{3}{20}$ $\frac{1}{20}$) | +0.1 | 2.34 | 1.05 | DB:2 |
| | | $\Sigma=5$ boundary of 53.1° | | | |
| Trans. 1 | (0.0, 0.0) | +0.0 | 2.99 | 1.16 | DB:2, FB:2 |
| Trans. 2 | ($\frac{1}{20}$, 0.0) | +0.7 | 2.69 | 0.93 | DB:4, TD:2 |
| Trans. 3 | ($\frac{1}{10}$, 0.0) | +0.5 | 2.69 | 1.12 | DB:2 |
| Trans. 4 | (0.0, $\frac{1}{20}$) | +0.2 | 2.80 | 1.08 | FB:4 |
| Trans. 5 | ($\frac{1}{20}$, $\frac{1}{20}$) | +0.2 | 2.48 | 1.07 | DB:1, FB:1 |
| Trans. 6 | ($\frac{1}{10}$, $\frac{1}{20}$) | +0.1 | 2.56 | 0.72 | +9.7%, +53.1° |
| Trans. 7 | (0.0, $\frac{1}{10}$) | +0.2 | 2.70 | 1.12 | FB:4 |
| Trans. 8 | ($\frac{1}{20}$, $\frac{1}{10}$) | +0.2 | 2.76 | 1.17 | FB:4 |
| Trans. 9 | ($\frac{1}{10}$, $\frac{1}{10}$) | +0.1 | 2.48 | 1.26 | +14.7%, +50.1° |

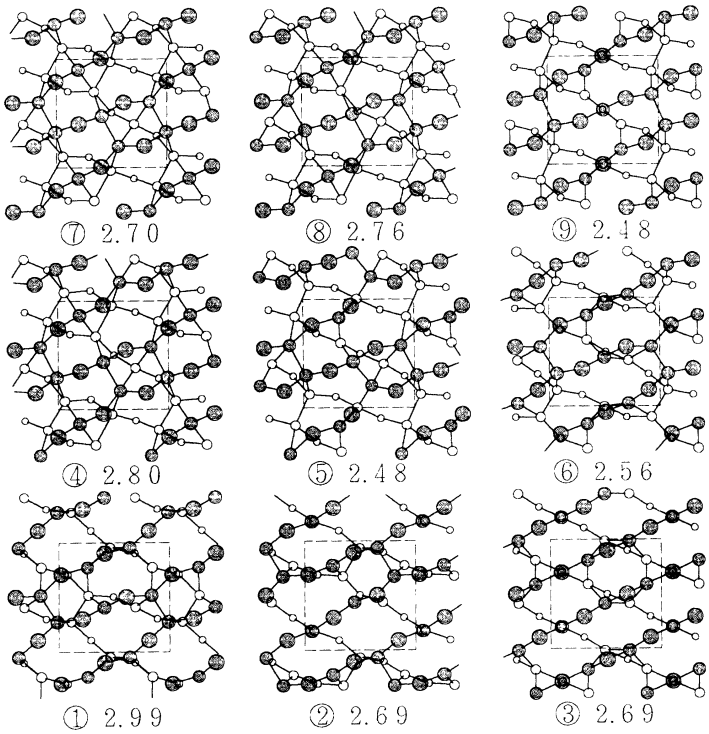


FIG. 11. Relaxed atomic configurations of the ⟨001⟩ $\Sigma=5$ twist boundary in Si with a rotation angle of 53.1°, against the rigid-body translations. The atomic configurations for the nine translations in the irreducible part of the DSC unit cell are shown by the same arrangement as the translations in Fig. 6(b). Interfacial energies of respective configurations are also shown in units of J/m$^2$.

interfacial and dimer bonds. For example, the configuration of Trans. 5 is constructed from that of Trans. 4 by breaking one dimer bond, one interfacial bond, and one back bond between the first and second layers in the CSL unit cell, and by forming one new interfacial bond. Thus the configuration of Trans. 5 contains three dimer bonds, one five-coordinated defect, and one three-coordinated defect at the second layer in the CSL unit cell. The configuration of Trans. 6 is generated from that of Trans. 5 by breaking one dimer bond and two interfacial bonds and by forming two interfacial bonds and one back bond, which eliminates all the coordination defects. The configuration of Trans. 9 is formed from that of Trans. 6 by switching two interfacial bonds in the CSL unit cell.

In both the boundaries, the configurations are very complex, and it seems that there exist no sharp or deep energy minima against the rigid-body translations. The configurations of Trans. 5 and Trans. 1 for the boundary of 36.9°, and those of Trans. 5 and Trans. 9 for the boundary of 53.1°, seem to be relatively stable. However, the reason why these configurations are relatively stable is not so clear compared with the shallow energy minima observed in the ⟨111⟩ $\Sigma=7$ and ⟨011⟩ $\Sigma=3$ boundaries. There exists no clear tendency for the energies and atomic structures against the translations, which is very different from the other twist boundaries. Thus it might be possible that other stable configurations with different bonding networks are generated for other values of translations normal to the interface.

In order to examine relatively stable configurations, we have performed the relaxation of the 140-atom cell of the boundary of 36.9° with Trans. 5 and the optimized translation normal to the interface, +0.08 Å. We have obtained a configuration with no coordination defects but with a bonding network different from that of Trans. 5 by the 60-atom cell shown in Fig. 10 in spite of the small difference in the translation normal to the interface. However, the energy and bond distortions are still very large. $E_{gb}$ is 2.05 J/m$^2$, and the bond-length and bond-angle distortions range from −2.5 to +16.0% and −24.4° to +37.3°, respectively. The energy per boundary atom is 0.9 eV, which is much larger than those of the ⟨111⟩ $\Sigma=7$ and ⟨011⟩ $\Sigma=3$ boundaries. Compared with the configuration of Trans. 5 by the 60-atom cell, the large bond-angle distortions over +50° are eliminated by switching two dimer bonds and two interfacial bonds in the unit cell. However, very large bond-length distortions over +16% are introduced. The $E_F$ of this configuration is 0.22 eV. The large bond distortions of this configuration generate empty deep states in the band gap.

We have also performed the relaxation of the 140-atom cell of the boundary of 36.9° with Trans. 2 and the optimized translation normal to the interface, +0.40 Å. The configuration obtained has a different bonding network from that of Trans. 2 by the 60-atom cell. In this configuration, the three-coordinated atom in the lower crystal in the CSL unit cell shown in Fig. 10 is eliminated by forming one interfacial bond, which results in the formation of one five-coordinated atom in the upper crystal in the unit cell. The $E_{gb}$ of this configuration is 2.08 J/m$^2$, which is similar to the value of Trans. 5 above.

It seems that different translations normal to the interface or different sizes of supercells generate various configurations with different bonding networks for the same translation parallel to the interface. These results indicate the possibility that there exist many metastable

configurations with different bonding networks for respective translations parallel to the interface, and that there exist many configurations with similar energies for different translations.

It is clear that the ⟨001⟩ $\Sigma=5$ twist boundaries in Si have special complex features as compared with other twist boundaries, such as complex configurations without clear energy minima against the translations, many metastable configurations with different bonding networks in a similar energy range, and very large interfacial energies with coordination defects or large bond distortions. These features of the ⟨001⟩ $\Sigma=5$ boundaries in Si are essentially similar to those found in the same boundaries in Ge in Ref. 32. Many configurations shown in Figs. 10 and 11 seem to resemble those of Ge in Ref. 32. Of course, detailed structures, numbers of coordination defects, and features of energy values are different from those in Ref. 32, because of the differences in materials, the definition of the coordination, the translations normal to the interface, and the method of calculations.

These complex features of the $\Sigma=5$ boundaries can be explained by the morphology of the ideal (001) surface. In the ideal (001) surface, respective surface atoms contain two dangling bonds pointing to different directions in contrast to one dangling bond per surface atom in the ideal (111) and (011) surfaces. This problem causes a much larger density of dangling bonds per surface area than those of the ideal (111) and (011) surfaces, and increases the difficulty in constructing stable configurations with as many dangling bonds reconstructed as possible, which should result in large interfacial energies with coordination defects or large bond distortions. This problem also provides a very high degree of freedom to construct various configurations through the formation of dimer bonds or interfacial bonds, which should result in a large variety of metastable configurations.

## V. DISCUSSION

Concerning the comparison with the results in Ref. 30 using the Stillinger-Weber potential, we also performed relaxations of the present boundaries by using the Stillinger-Weber potential. It has been found that the Stillinger-Weber potential tends to generate more five-coordinated defects and to give smaller energy values for disordered structures, especially containing five-coordinated defects, as compared with the present method. This tendency was observed in calculations of amorphous Si.[47,48] This is caused by the unrealistic energy decreases associated with overcoordinated defects by the two-body function in the Stillinger-Weber potential not properly supplemented by the increases in the three-body function. We have found that the interfacial energies of the ⟨111⟩ $\Sigma=7$ boundaries are estimated to be much smaller by the Stillinger-Weber potential, as reported in Ref. 30, than the present values. This is also caused by the unrealistic energy decreases due to the two-body function in the Stillinger-Weber potential, because there exist many atoms facing each other within the interaction distance of about 3.8 Å of the Stillinger-Weber potential at the interfaces of the ⟨111⟩ twist boundaries.

By the present calculations, it has been shown that twist boundaries with three types of rotation axes and boundary planes have different features of energies and atomic structures, respectively. The ⟨001⟩ $\Sigma=5$ boundaries have very complex configurations with very large energies, and with many coordination defects or very large bond distortions. There exist many metastable configurations in a similar energy range, and no clear energy minima against the translations. On the other hand, the configurations of the ⟨111⟩ $\Sigma=7$ and ⟨011⟩ $\Sigma=3$ twist boundaries are not so complicated. There exist certain tendencies of the energies and configurations against the rigid-body translations, and relatively stable configurations without any coordination defects can be constructed. The different features among these twist boundaries can be explained by the morphology of respective ideal surfaces, as discussed in Sec. IV.

However, even in the cases of the ⟨111⟩ $\Sigma=7$ and ⟨011⟩ $\Sigma=3$ twist boundaries, it should be noted that the bond distortions and interfacial energies of the most stable configurations are still much larger than those of the tilt boundaries. Such configurations exist not at sharp or deep energy minima but only at shallow energy minima against the rigid-body translations, differently from the tilt boundaries.

Thus the present results clearly indicate the possibility that twist boundaries generally contain greater structural disorder and larger interfacial energies than tilt boundaries in Si. This point also has been discussed in the theoretical study of the comparison between ⟨001⟩ twist and ⟨001⟩ tilt boundaries in Ge.[33] For twist boundaries, it does not seem to be easy to construct stable configurations without any large bond distortions or coordination defects, and with sharp or deep energy minima against the rigid-body translations like those of the tilt boundaries, at least when they are constructed by ideal surfaces.

Of course, it might be possible to construct more stable configurations for the present twist boundaries by introducing point defects, by destroying the symmetrical properties, or by introducing a large-scale reconstruction beyond the CSL unit cells or beyond several atomic layers. However, for twist boundaries, it does not seem to be easy to construct stable configurations like those of the tilt boundaries from the viewpoint of the structural units. In stable configurations of the tilt boundaries in Si or Ge, interfaces are constructed by arranging structural units consisting of atomic rings such as five-, six-, and seven-membered rings without any large bond distortions or coordination defects. It should be noted that this is a general feature of stable configurations for extended defects in Si or Ge, such as dislocation cores, stacking faults, or {113} planar interstitial defects, in addition to tilt boundaries, as discussed in Ref. 50. In the cases of twist boundaries, such types of stable structural units cannot easily be constructed, which causes greater structural disorder and larger interfacial energies for the present twist boundaries. This is the reason why twist boundaries are seldom found in polycrystalline Si or Ge as compared with the tilt boundaries.

Of course, the observed predominance of the ⟨011⟩ tilt boundaries in polycrystalline Si (Ref. 51) or Ge should be related not only to the interfacial energies, but also to the process of the formation of grain boundaries. It is probable that various ⟨011⟩ tilt boundaries are formed through faceting or splitting[9,51] after preferential formation of special stable interfaces such as {111} $\Sigma=3$ tilt boundaries or {111} stacking faults with very low interfacial energies.[16] We believe this point is the reason why other types of tilt boundaries such as ⟨001⟩ tilt boundaries are seldom found in polycrystalline Si. However, we believe the primary reason why twist boundaries are seldom found is their high interfacial energies. Concerning this point, it is not impossible that several twist boundaries are generated through faceting or splitting from special stable interfaces, at least crystallographically. For example, as can be seen in Fig. 9, the interface of the {111} $\Sigma=3$ tilt boundary can be introduced perpendicularly to the configuration of Trans. 1 of the ⟨011⟩ $\Sigma=3$ twist boundary along the $[2,-1,1]$ direction. Also, the interface of the {211} $\Sigma=3$ tilt boundary can be introduced perpendicularly to the ⟨011⟩ $\Sigma=3$ twist boundary along the $[-1,-1,1]$ direction. Thus the $\Sigma=3$ boundary in Si seems to exhibit faceting on the {111} and {011} or {211} and {011} planes, as well as the {111} and {211} planes.[27] However, the $\Sigma=3$ boundary observed shows faceting only on the {111} and {211} planes, and no facets or steps on the {011} plane have been observed in Si or Ge. In other words, the faceted $\Sigma=3$ boundaries are all tilt boundaries on the {111} or {211} planes, and do not contain ⟨011⟩ twist boundaries on the {011} plane. We believe this is caused mainly by the large interfacial energy of the ⟨011⟩ $\Sigma=3$ twist boundary as compared with the {111} and {211} interfaces of the tilt boundaries,[16,18] as is shown in the present calculations.

Finally, the present results indicate that the disordered configurations of the twist boundaries can be regarded as models of local configurations of general disordered boundaries, which are related to the observed band tails or midgap states in polycrystalline Si. The present twist boundaries contain shallow or deep states inside the minimum band gap in contrast to the tilt boundaries. Thus it is of much interest to investigate the electronic structures of such disordered configurations. This should contribute to an understanding of the origins of the gap states observed at grain boundaries in Si. Detailed analyses will be given in our following papers.

## VI. CONCLUSION

The overall features of energies and atomic structures at twist boundaries in Si with different rotation axes and boundary planes—the ⟨111⟩ $\Sigma=7$, ⟨011⟩ $\Sigma=3$, and ⟨001⟩ $\Sigma=5$ twist boundaries—have been examined by using the transferable SETB method. The results have been compared with those of the tilt boundaries in Si. It has been shown that twist boundaries contain larger bond distortions or more coordination defects, and much larger interfacial energies than those of the tilt boundaries. It does not seem that deep or sharp energy minima exist against rigid-body translations for the twist boundaries. About the ⟨111⟩ $\Sigma=7$ and ⟨011⟩ $\Sigma=3$ boundaries, configurations without any coordination defects can be constructed for proper translations as well as for the tilt boundaries. However, these contain larger bond distortions and much larger interfacial energies than those of the tilt boundaries, and contain shallow states in the band gap. The ⟨011⟩ $\Sigma=5$ boundaries have very complex structures and much larger interfacial energies than the other twist boundaries, and frequently contain coordination defects and deep states in the band gap. The different features of the respective twist boundaries can be explained by the morphology of the respective ideal surfaces. It can be said that stable structural units consisting of atomic rings without any large bond distortions or coordination defects similar to those in the tilt boundaries are difficult to construct for the twist boundaries in Si. This is the reason why twist boundaries are seldom found in polycrystalline Si as compared with the frequently observed tilt boundaries.

## ACKNOWLEDGMENTS

The authors are grateful to Professor Y. Ishida for helpful discussions and encouragement. The present study was supported by the Science and Technology Agency of Japan as the project "Materials Interconnection."

[1]See papers in *Polycrystalline Semiconductors,* edited by H. J. Möller, H. P. Strunk, and J. H. Werner, Springer Proceedings in Physics Vol. 35 (Springer, Berlin, 1989); *Polycrystalline Semiconductors II,* edited by J. H. Werner and H. P. Strunk, Springer Proceedings in Physics Vol. 54 (Springer, Berlin, 1991); *Polycrystalline Semiconductors III,* edited by H. P. Strunk, J. H. Werner, O. Bonnaut, and B. Fortin (Trans Tech, Brookfield, MA, in press).

[2]See papers in *Intergranular and Interphase Boundaries in Materials,* edited by Ph. Komninou and A. Rocher, Materials Science Forum Vols. 126–128 (Trans Tech, Brookfield, MA, 1993).

[3]W. Bollmann, *Crystal Defects and Crystalline Interfaces* (Springer, Berlin, 1970).

[4]A. P. Sutton, in *Polycrystalline Semiconductors II* (Ref. 1), p. 116.

[5]J. Thibault, J. L. Rouviere, and A. Bourret, in *Materials Science and Technology,* edited by R. W. Cahn, P. Haasen, and E. J. Kramer (VCH, Weinheim, 1991), Vol. 4, p. 321.

[6]L. K. Fionova and A. V. Artemyev, *Grain Boundaries in Metals and Semiconductors* (Les Editions de Physique, Les Ulis, 1993).

[7]O. L. Krivanek, S. Isoda, and K. Kobayashi, Philos. Mag. **36,** 931 (1977).

[8]M. D. Vaudin, B. Cunningham, and D. G. Ast, Scr. Met. **17**, 191 (1983).
[9]A. Bourret and J. J. Bacmann, Suf. Sci. **162**, 495 (1985); Trans. Jpn. Inst. Met. Suppl. **27**, 125 (1986).
[10]J. Thibault-Desseaux and J. L. Putaux, in *Structure and Properties of Dislocations in Semiconductors 1989,* edited by S. G. Roberts, D. B. Holt, and P. R. Wilshaw, IOP Conf. Proc. No. 104 (Institute of Physics, Bristol, 1989), p. 1.
[11]A. Bourret and J. L. Rouviere, in *Polycrystalline Semiconductors* (Ref. 1), p. 8.
[12]Y. Ishida and H. Ichinose, in *Polycrystalline Semiconductors* (Ref. 1), p. 42.
[13]M. Kohyama, R. Yamamoto, and M. Doyama, Phys. Status Solidi B **137**, 11 (1986); **138**, 387 (1986); M. Kohyama, *ibid.* **141**, 71 (1987).
[14]A. P. Sutton and V. Vitek, Philos. Trans. R. Soc. London Ser. A **309**, 1 (1983).
[15]R. E. Thomson and D. J. Chadi, Phys. Rev. B **29**, 889 (1984).
[16]A. T. Paxton and A. P. Sutton, J. Phys. C **21**, L481 (1988); Acta Metall. **37**, 1693 (1989).
[17]M. Kohyama, R. Yamamoto, Y. Ebata, and M. Kinoshita, J. Phys. C **21**, 3205 (1988).
[18]M. Kohyama, R. Yamamoto, Y. Watanabe, Y. Ebata, and M. Kinoshita, J. Phys. C **21**, L695 (1988).
[19]M. Kohyama, S. Kose, M. Kinoshita, and R. Yamamoto, J. Phys. Condens. Matter **2**, 7809 (1990).
[20]D. P. DiVincenzo, O. L. Alerhand, M. Schlüter, and J. W. Wilkins, Phys. Rev. Lett. **56**, 1925 (1986).
[21]A. V. Nikolaeva, A. V. Artemyev, Yu. H. Vekilov, L. K. Fionova, and M. B. Samsonova, J. Phys. Condens. Matter **4**, 2775 (1992).
[22]T. A. Arias and J. D. Joannopoulos, Phys. Rev. Lett. **69**, 3330 (1992); Phys. Rev. B **49**, 4525 (1994).
[23]J. Werner and M. Peisl, Phys. Rev. B **31**, 6881 (1985).
[24]A. J. Madenach and J. H. Werner, Phys. Rev. B **38**, 13 150 (1988).
[25]J. H. Werner, in *Structure and Properties of Dislocations in Semiconductors 1989* (Ref. 10), p. 63.
[26]D. Jousse, S. L. Delage, and S. S. Iyer, Philos. Mag. B **63**, 443 (1991).
[27]M. Kohyama, S. Kose, M. Kinoshita, and R. Yamamoto, J. Phys. Condens. Matter **1**, 8251 (1989).
[28]J.-L. Maurice, in *Polycrystalline Semiconductors II* (Ref. 1), p. 166.
[29]M. Kohyama, R. Yamamoto, and M. Doyama, Phys. Status Solidi B **136**, 31 (1986).
[30]S. R. Phillpot and D. Wolf, Philos. Mag. A **60**, 545 (1989).
[31]F. H. Stillinger and T. A. Weber, Phys. Rev. B **31**, 5262 (1985).
[32]E. Tarnow, P. Dallot, P. D. Bristowe, J. D. Joannopoulos, G. P. Francis, and M. C. Payne, Phys. Rev. B **42**, 3644 (1990).
[33]E. Tarnow, T. Arias, P. D. Bristowe, P. Dallot, G. P. Francis, J. D. Joannopoulos, and M. C. Payne, in *Atomic Scale Calculations of Structure in Materials,* edited by M. S. Daw and M. A. Schlüter, MRS Symposia Proceedings No. 193 (Materials Research Society, Pittsburgh, 1990), p. 235.
[34]S. Sawada, Vacuum **41**, 612 (1990).
[35]M. Kohyama, J. Phys. Condens. Matter **3**, 2193 (1991).
[36]D. J. Chadi, Phys. Rev. Lett. **41**, 1062 (1978); Phys. Rev. B **29**, 785 (1984); A. T. Paxton, A. P. Sutton, and C. M. M. Nex, J. Phys. C **20**, L263 (1987).
[37]Preliminary accounts about the electronic structures of the twist boundaries have been given by M. Kohyama, S. Kose, and R. Yamamoto, in *Defect Engineering in Semiconductor Growth, Processing and Device Technology,* edited by S. Ashok, J. Chevallier, K. Sumino, and E. Weber, MRS Symposia Proceedings No. 262 (Materials Research Society, Pittsburgh, 1992), p. 567; M. Kohyama and R. Yamamoto, in *Amorphous Silicon Technology—1993,* edited by E. A. Schiff, M. J. Thompson, A. Madan, K. Tanaka, and P. G. LeComber, MRS Symposia Proceedings No. 297 (Materials Research Society, Pittsburgh, 1993), p. 177.
[38]L. Goodwin, A. J. Skinner, and D. G. Pettifor, Europhys. Lett. **9**, 701 (1989).
[39]J. Robertson, Philos. Mag. B **47**, L33 (1983).
[40]K. C. Pandey and J. Phillips, Phys. Rev. Lett. **32**, 1433 (1974); Phys. Rev. B **13**, 750 (1976).
[41]D. J. Chadi and M. L. Cohen, Phys. Rev. B **8**, 5747 (1973).
[42]M. T. Yin and M. L. Cohen, Phys. Rev. B **29**, 6996 (1984).
[43]D. Tomanek and M. A. Schlüter, Phys. Rev. Lett. **56**, 1055 (1986); Phys. Rev. B **36**, 1208 (1987).
[44]W. M. C. Foulkes and R. Haydock, Phys. Rev. B **39**, 12 520 (1989).
[45]A. P. Sutton, M. W. Finnis, D. G. Pettifor, and Y. Ohta, J. Phys. C **21**, 35 (1988).
[46]H. J. Monkhorst and J. D. Pack, Phys. Rev. B **13**, 5188 (1976).
[47]M. D. Kluge, J. R. Ray, and A. Rahman, Phys. Rev. B **36**, 4234 (1987).
[48]W. D. Luedtke and U. Landman, Phys. Rev. B **40**, 1164 (1989).
[49]D. A. Drabold, P. A. Fedders, O. F. Sankey, and J. D. Dow, Phys. Rev. B **42**, 5135 (1990).
[50]M. Kohyama and S. Takeda, Phys. Rev. B **46**, 12 305 (1992).
[51]A. Garg, W. A. T. Clark, and J. P. Hirth, Philos. Mag. A **59**, 479 (1989).

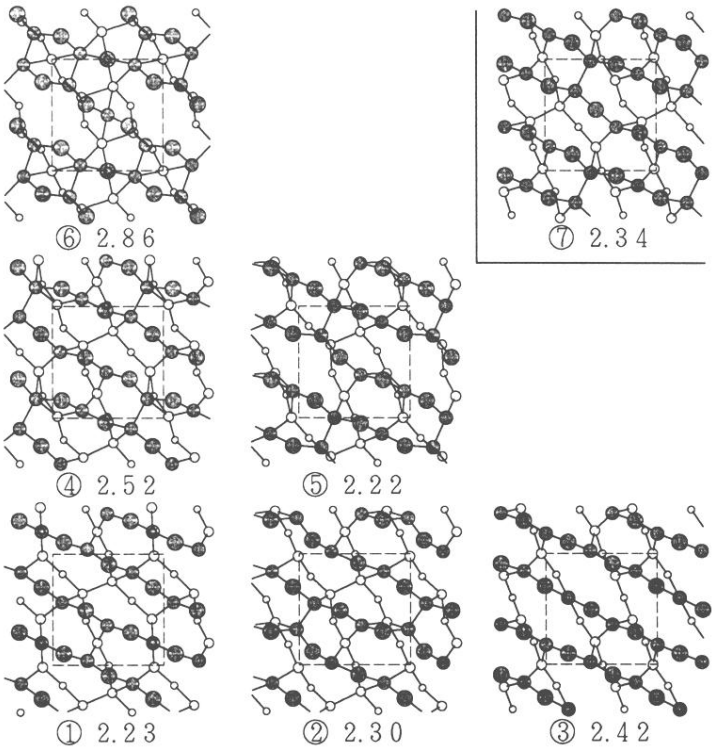


FIG. 10. Relaxed atomic configurations of the ⟨001⟩ $\Sigma=5$ twist boundary in Si with a rotation angle of 36.9°, against the rigid-body translations. The atomic configurations for the seven translations in the irreducible part of the DSC unit cell are shown by the same arrangements as the translations in Fig. 6(a), with the exception of the enclosed structure of Trans. 7. Interfacial energies of respective configurations are also shown in units of $J/m^2$.

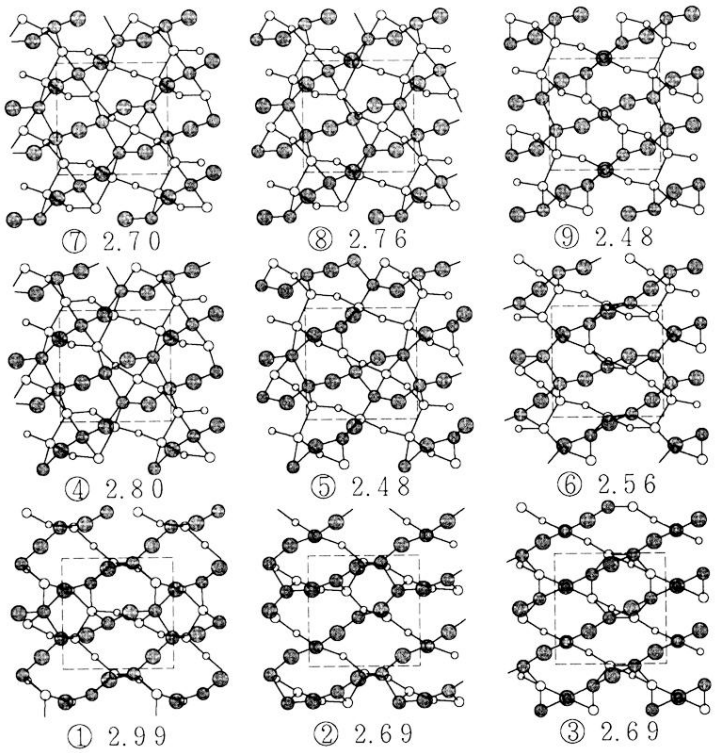


FIG. 11. Relaxed atomic configurations of the $\langle 001 \rangle$ $\Sigma = 5$ twist boundary in Si with a rotation angle of 53.1°, against the rigid-body translations. The atomic configurations for the nine translations in the irreducible part of the DSC unit cell are shown by the same arrangement as the translations in Fig. 6(b). Interfacial energies of respective configurations are also shown in units of $J/m^2$.

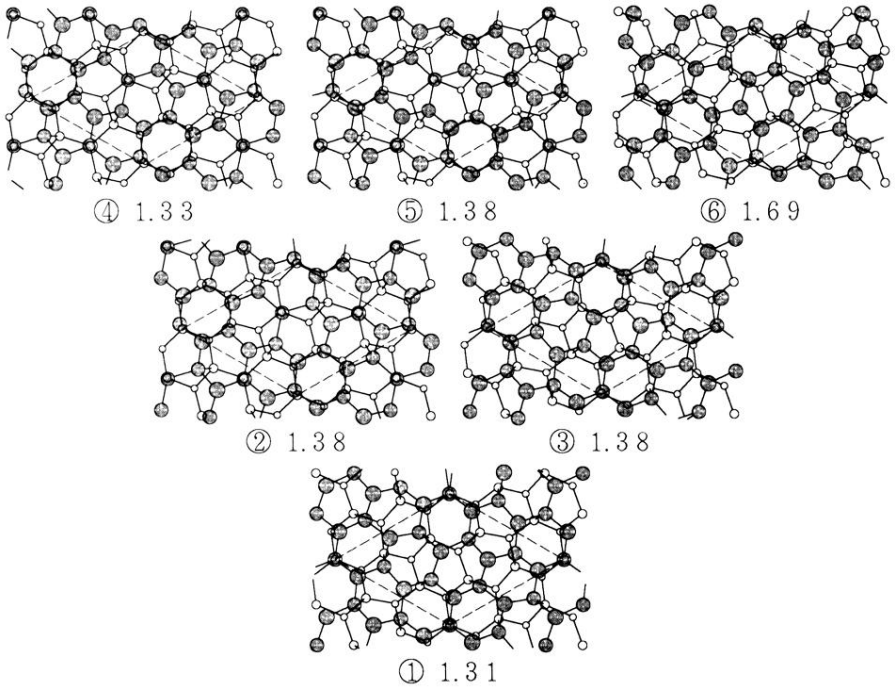


FIG. 7. Relaxed atomic configurations of the ⟨111⟩ $\Sigma=7$ twist boundary in Si with a rotation angle of 38.2°, against the rigid-body translations. The atomic configurations for the six translations in the irreducible part of the DSC unit cell are shown by the same arrangement as the translations in Fig. 4(a). Interfacial energies of respective configurations are also shown in units of $J/m^2$.

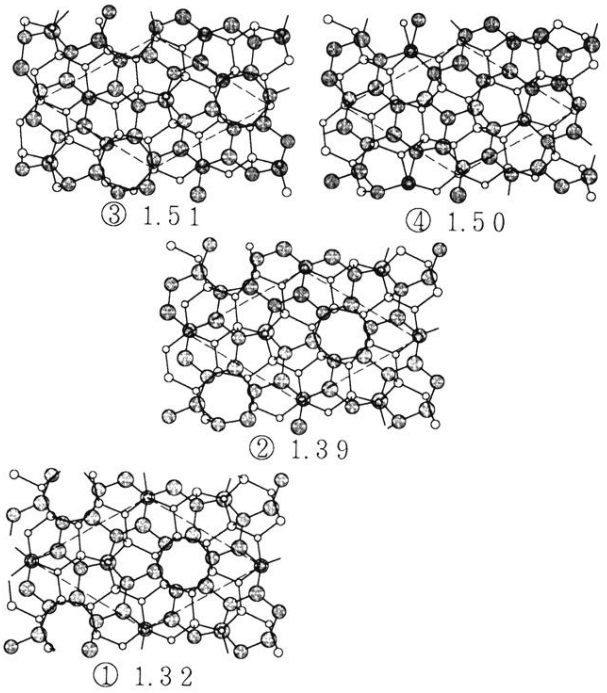


FIG. 8. Relaxed atomic configurations of the ⟨111⟩ $\Sigma=7$ twist boundary in Si with a rotation angle of 98.2°, against the rigid-body translations. The atomic configurations for the four translations in the irreducible part of the DSC unit cell are shown by the same arrangement as the translations in Fig. 4(b). Interfacial energies of respective configurations are also shown in units of $J/m^2$.

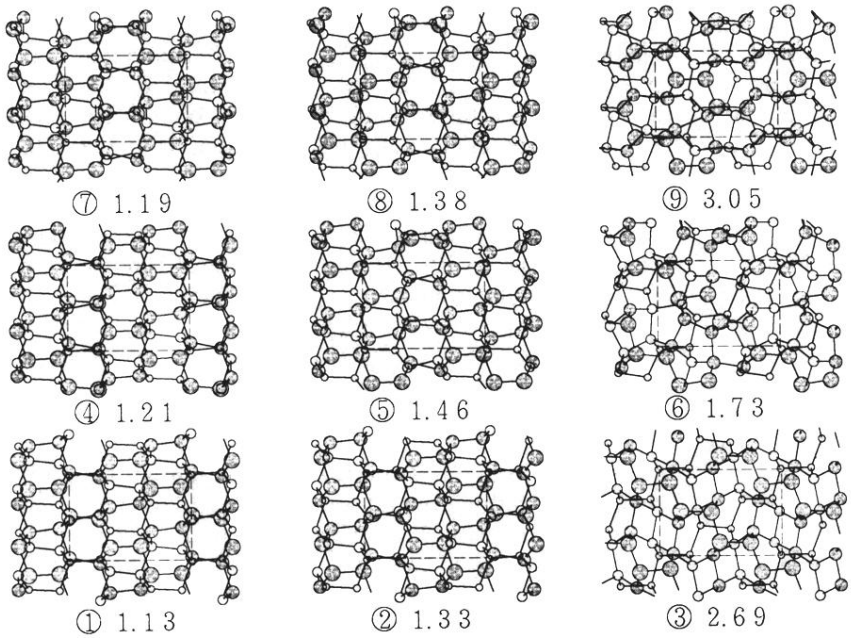


FIG. 9. Relaxed atomic configurations of the ⟨011⟩ $\Sigma=3$ twist boundary in Si with a rotation angle of 109.5°, against the rigid-body translations. The atomic configurations for the nine translations in the irreducible part of the DSC unit cell are shown by the same arrangement as the translations in Fig. 5. Interfacial energies of respective configurations are also shown in units of $J/m^2$.